RSC Advances

ROYAL SOCIETY OF CHEMISTRY

www.rsc.org/advances

RSC Advances

An international journal to further the chemical sciences

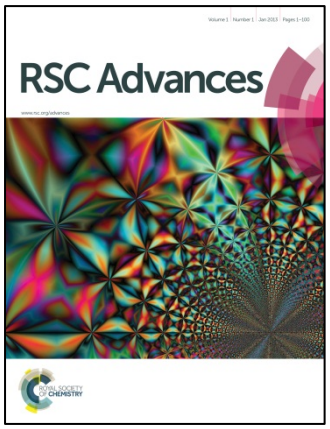

RSC Advances is an international, peer-reviewed, online journal covering all of the chemical sciences, including interdisciplinary fields.

The **criteria for publication** are that the experimental and/ or theoretical **work must be high quality, well conducted adding to the development of the field**.

RSC Advances* has a 2012 partial impact factor of 2.56

Thank you for your assistance in evaluating this manuscript.

Guidelines to the referees

Referees have the responsibility to treat the manuscript as confidential. Please be aware of our Ethical Guidelines, which contain full information on the responsibilities of referees and authors, and our Refereeing Procedure and Policy.

It is essential that all research work reported in *RSC Advances* is well-carried out and well-characterised. There should be enough supporting evidence for the claims made in the manuscript.

When preparing your report, please:

- comment on the originality and scientific reliability of the work;
- comment on the characterisation of the compounds/materials reported - has this has been accurately interpreted and does it support the conclusions of the work;
- state clearly whether you would like to see the article accepted or rejected and give detailed comments (with references, as appropriate) that will both help the Editor to make a decision on the article and the authors to improve it.

Please inform the Editor if:

- there is a conflict of interest
- there is a significant part of the work which you are not able to referee with confidence
- the work, or a significant part of the work, has previously been published
- you believe the work, or a significant part of the work, is currently submitted elsewhere
- the work represents part of an unduly fragmented investigation.

For further information about *RSC Advances*, please visit: www.rsc.org/advances or contact us by email: advances@rsc.org.

*Data based on 2012 Journal Citation Reports®, (Thomson Reuters, 2013).

RSC Advances

RSCPublishing

Plasmonic Cavities Derived from the Silver Nanoparticles atop the Massed Silver Surface for Surface Enhancement Raman Scattering

Cite this: DOI: 10.1039/x0xx00000x

Received ooth July 2014,
Accepted ooth oo 2014

DOI: 10.1039/x0xx00000x

www.rsc.org/

Shu-Chun Cheng [a], Ten-Chin Wen*[a b], and Yung-Chiang Lan *[c]

Various plasmonic cavities (PC) are formed by positioning silver nanocubes or nanospheres on the massed silver surface, being magnificently useful for surface enhancement Raman scattering (SERS) application. In this case, a red-shift in wavelength of surface plasmon resonance (SPR) increases with the decrease in gap width according to the simulation results of absorption spectra by finite-difference time-domain method. Nanocube-insulator-metal geometry with the 2 nm gap width (2-NcIM) possesses the strong electromagnetic (EM) field distribution and its PC forms near 633 nm radiation. In order to validate the simulation results, two geometries were selected for SERS experiments by using rhodamine 6G (R6G) as model compound with 633 nm laser irradiation. To our surprise, 2-NcIM possesses respectively 2.06×10^4 and 2.41×10^4 times experimental and simulated enhancement factors (EFs) of nanosphere-insulator-metal geometry with the 2 nm gap width ($1.5 \pm 0.25\times10^4$ and 4.82×10^4), confirming the validity of the simulation results. It also prompts us not only to clarify the role of our special substrates in extra high EF for SERS application but also to design the innovative, highly sensitive, and low cost substrates via the simulation results.

Introduction

Surface plasmon resonance (SPR) is triggered by the coherent oscillations of free electrons at metal-dielectric interface with the excitation by electromagnetic (EM) wave irradiation [1, 2]. This unique property had been extensively studied for signal amplification applications, such as waveguides [3], reflectors [4], splitters [5] and shows high potential application in Surface Enhanced Raman Scattering (SERS) [6-8]. The SPR wavelengths of noble metals (Al, Ag, and Au) nanoparticles are in the region of visible light, which is suitable to enhance Raman signals due to the match with the common used 532, 633, and 780 nm lasers [9-11]. The coupling between two metal nanoparticles at the nanogaps to resonate the plasmons at the interfaces of metals, which is called plasmonic cavity (PC), leading to the strong SPR had been investigated and widely applied to SERS [12-15]. However, it is hard to create high density of SPR via this method due to the difficulty in decreasing the gap width with the extremely low value. Recently, various geometries of metal nanoparticles atop the massed metal surfaces with ultrathin insulators as the gaps (NpIM) have been extensively studied both theoretically [16-17] and experimentally [12-15] due to the ease to create large area and high density of SPR. NpIM with geometry of gold nanospheres atop the massed gold surface had been used as a convenient and highly sensitive SERS sensor for detection of biomolecules by S. Mahajan *et al* [18]. Xia et al. also demonstrated that high enhancement factor (EF) can be achieved with a silver nanocubes atop the silver film geometry using chemical synthesized SiO_2 around the silver nanocubes as the insulator [19]. C. J. Murphy *et al.* used self-assembled analyte around the gold nanocubes atop the gold surface as the substrates to get the extremely high EF for detecting 4-mercaptobenzoic acid [20]. The silver nanocubes atop the silver surface functionized by 1, 2-ethanedithiol monolayer as the insulator had been found to effectively enhance the rhodamine 6G (R6G) siganls [21].

In addition to the strong SPR created by PC, the gap width and shape of metal nanoparticels are also important to vary the intensity and resonance wavelength of SPR. K. D. Alexander *et al.* had found the high SERS signals can be achieved via adjusting the interdistance between gold nanorods [22]. The effect of various gap width between the silver nanocubes on the shift of SPR wavelength and the calculated SERS EFs had been studied by O. Rabin *et al* [23]. Shapes of gold nanoparticles dependence of SERS detecting had been investigated by C. J. Murphy *et al* [24]. However, the systematical investigation of gap width and shape of nanoparticles effects on PC in the NpIM geometry have not been investigated. In this study, the simulated absorption spectra and the EM field density diagrams of the silver nanocubes atop the massed silver surface with the air as insulator (NcIM) with 2, 3, 4, 5, and 10 nm gap width under the wavelength of maximum absorbance (λ_{max}) and 633 nm lasers irradiation were simulated via finite difference time domain (FDTD) method to investigate the role of gap width in

the PC of the NcIM. The comparisons between simulation and experiment results of NcIM and the silver nanosphere atop the massed silver surface with the air as insulator (NsIM) were also conducted to understand the shape effect on PC and the SERS performance.

Results and discussion

The simulated absorption spectra of the NcIM with 2, 3, 4, 5, and 10 nm gap width (denoted as 2-NcIM, 3-NcIM, 4-NcIM, 5-NcIM, and 10-NcIM) are shown in Fig. 1. The inset shows the scheme of NcIM geometry with 50 nm sized silver nanocubes under the polarized laser irradiation with the direction vertically downward. NcIM with 1 nm gap width is beyond the discussion due to the high technical difficulty in fabricating such substrate. The absorption peaks below 450 nm are denoted as the high order mode except for the second peak of 10-NcIM. The simulated adsorption peaks at 670, 577, 526, 493, and 420 nm respectively for 2-NcIM, 3-NcIM, 4-NcIM, 5-NcIM, and 10-NcIM are the PC mode, resulting from the coupling of surface plasmons at nanoparticle and propagating surface plasmons on the massed silver surface. The absorbance intensity increases with the decrease in gap width of NcIM, showing the stronger plasmon coupling between silver nanocubes and surface with the smaller gap width. The redshift of PC mode increases with the decrease in the gap width of NcIM, which is consistent with the result of dispersion relation of metal-insulator-metal (MIM) geometry that shows the resonance frequency at the same wave vector decreases with the decrease in the gap width of MIM. The redshift of PC mode means that the PC of NcIM with smaller gap width should be excited under the longer wavelength laser irradiation to get the maximum resonance.

The EM field densities in X-Z plane of 2-NcIM, 3-NcIM, 4-NcIM, 5-NcIM, and 10-NcIM under the λ_{max} laser irradiation are shown Fig. 2a. The area of the strong EM density decreases with the increase of the gap width in the NcIM geometry, which is consistent with the intensity in the simulated absorption spectra. The smaller intensity of PC results from weaker

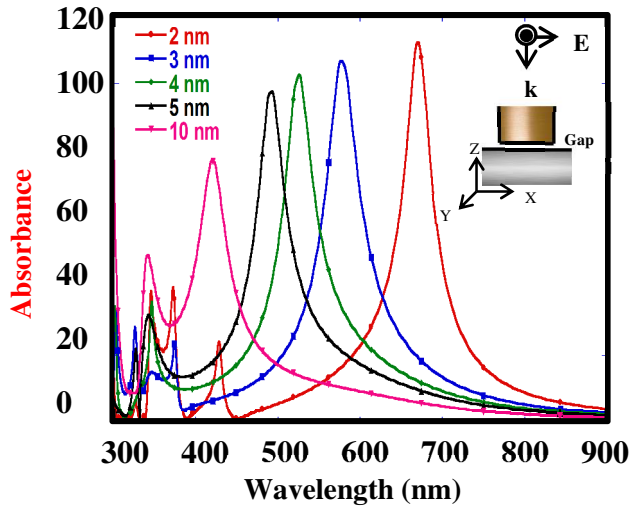

Fig. 1 The simulated absorption spectra for the NcIM with 2, 3, 4, 5, and 10 nm gap. Note: The absorbance is calculated from the ratio of the EM field amplitude with substrate to that of background (without substrate).

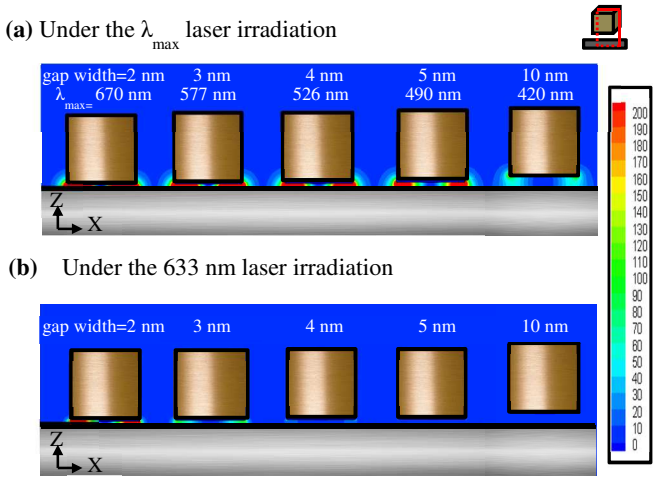

Fig. 2 The EM field densities of 2-NcIM, 3-NcIM, 4-NcIM, 5-NcIM, and 10-NcIM in X-Z plane under (a) the λ_{max} laser irradiation and (b) the 633 nm laser irradiation.

coupling of surface plasmons at nanoparticle with propagating surface plasmons on the massed silver surface with the larger gap width. Especially, the EM field density in 10-NcIM is concentrated at the corners of the cube, showing the resonance is weaker for the coupling between silver surfaces than the sharp corner effect of silver nanocubes. In spite of the strong EM density enhancement from PC under λ_{max} laser irradiation, these wavelengths mismatch the common used laser wavelength (633 nm) to induce such strong resonance. The EM field densities of NcIMs under the 633 nm laser irradiation were simulated as shown in Fig. 2b. The EM field intensity of PC in 2-NcIM is stronger than 3-NcIM owing to the smaller deviation between λ_{max} and 633 nm for 2-NcIM ($37 = 670 (\lambda_{max}) - 633$ nm) than 3-NcIM ($56 = 633 - 577 (\lambda_{max})$ nm). The intensity of PC for 4-NcIM, 5-NcIM, and 10-NcIM is almost zero due to the large deviation between λ_{max} and 633 nm. According to the above results, the wavelength of PC should match the incident laser to induce strong resonance for SERS application. The 2 nm gap width was chosen for the discussion of shape effect of silver nanoparticles on SERS via simulation and experiments due to the closely match between its λ_{max} and 633 nm laser.

In order to investigate the shape effect of silver nanoparticles on PC, the simulated absorption spectra of silver nanocubes atop the massed silver surface without the insulator (denoted as NcM), 2-NcIM, and silver nanosphere with diameter of 50 nm atop the massed silver surfaces without and with 2 nm gap width (denoted as NsM and 2-NsIM) are shown in Fig. 3. Except 2-NcIM, all curves were multiplied by several times for the significant contrast. 2-NcIM possesses the stronger intensity of PC mode than NcM, NsM, and 2-NsIM, depicting that the stronger PC derived from the parallel silver surface than the curve silver surface. However, the intensity of PC mode at the 530 nm can be shown in NsM rather than 2-NsIM. This special behavior can be illustrated via the simulation of the EM field density of these four substrates. In the case of NcM, 2-NcIM, NsM, and 2-NsIM under the λ_{max} laser irradiation, the EM field densities in X-Z and X-Y plane are respectively shown in Fig. 4a and Fig. 4b. The larger area of EM density and the higher intensity of PC exist in 2-NcIM than NcM, NsM, and 2-NsIM, which is consistent with the results of simulated absorption spectra. Due to the direct contact between silver nanocubes and surface, there is no PC observed in NcM.

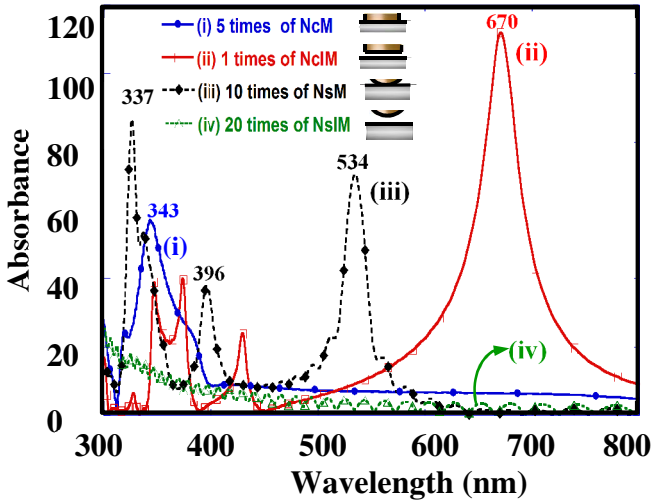

Fig. 3 The simulated absorption spectra for (i) 5 times the absorbance of NcM, (ii) 1 times the absorbance of NcIM, (iii) 10 times the absorbance of NsM and (iv) 20 times the absorbance of NsIM. Note: The observable waves of NsIM in (iv) are noises from Fourier transform.

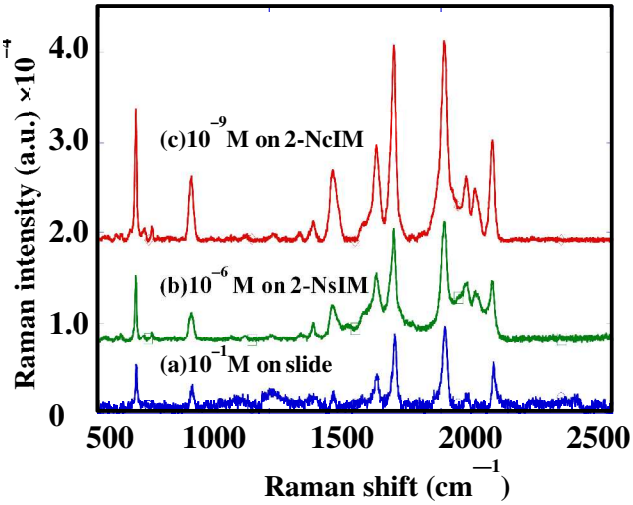

Fig.5 SERS spectra under the 633 nm laser irradiation for (a) 10^{-1} M R6G solution on microscope slide, (b) 10^{-6} M R6G solution on 2-NsIM, and (c) 10^{-9} M R6G solution on 2-NcIM.

At the center of silver nanosphere in NsM, the EM filed density is almost zero due to the direct contact. As the positon away from the center, the intensity will decrease, resulting from the increase in the gap width to lower the plasmon coupling between silver nanosphere and surface. The similar phenomena in 2-NsIM was also observed with the smaller intensity of EM field density. Accordingly, the intensity of PC will largely decay as the gap width larger than 2 nm. The higher EM field density and the larger extended PC area can be obtained due to the larger PC derived from the parallel silver surface than the curve silver surface.

In order to confirm the validity of the simulation results, we choose 2-NcIM and 2-NsIM for SERS experiments by using R6G as model compound. From our previous study [21], the gap width in the case of 50 nm silver nanocube self-assembled on the massed silver surface was estimated as 2 nm. It provides us a good chance to make a comparison between simulation results and SERS experiments. The Raman spectra for detecting R6G molecules of microscopic slide, 2-NsIM, and 2-NcIM under the 633 nm laser irradiation are shown in Fig. 4. The characteristic peaks of standard R6G signals can be observed in

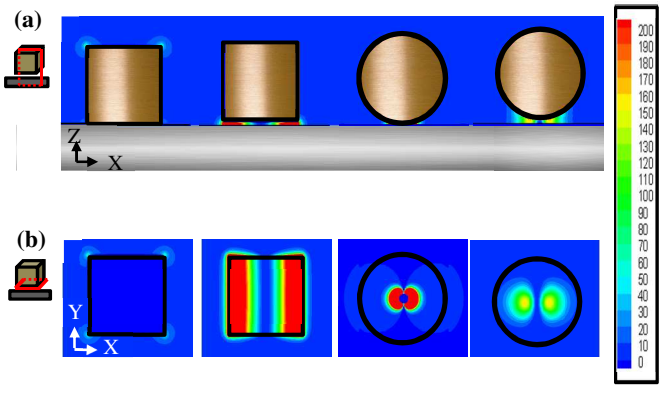

Fig. 4 The EM field densities of NcM, 2-NcIM, NsM and 2-NsIM at (a) X-Z plane in the middle of nanoparticle and (b) X-Y plane in the middle of nanogap.

the spectrum of microscopic slide, which is measured under the high R6G concentration (10^{-1} M) preventing the effect of noise signals. These R6G characteristic peaks with negligible noise signals are also shown in the spectra of 2-NsIM and 2-NcIM, depicting their high SERS sensitivity. The detection limits of microscopic slide, 2-NsIM, and 2-NcIM are 10^{-1}, 10^{-6}, and 10^{-9} M R6G solution, respectively. The lower detection limit of 2-NcIM than 2-NsIM represents the more R6G molecules detected due to the larger extended PC area for 2-NcIM than 2-NsIM. The high detection limit of microscopic slide comes from the lack of nanostructure to create SPR. The Raman intensity is higher for 2-NcIM than 2-NsIM at the lower R6G concentration due to the higher EM field density. In order to compare experimental results with the simulations, the experimental EFs and simulated EFs were respectively calculated according to Equations S1 and S2. (Supporting information) Table 1 shows that the experimental EFs and simulated EFs and are respectively 3.1×10^{8} and 1.16×10^{9} for 2-NcIM and 1.5×10^{4} and 4.82×10^{4} for 2-NsIM. The experimental EFs are statistically calculated from 20 different R6G signals at 1360 cm^{-1} using 95% confidence interval with t statistics. (Supporting information) Excitingly, 2NcIM possesses respectively 2.06×10^{4} and 2.41×10^{4} times experimental and simulated EFs of 2-NsIM ($1.5 \pm 0.25\times10^{4}$ and 4.82×10^{4}), confirming the validity of the simulation results. Combining the experimental and the simulation results, PC derived from the parallel silver surface possesses the higher EFs and the lower detection limit than the curve silver surface due to the higher EM field density and the larger extended PC

Table 1 The comparison of EFs between 2-NcIM and 2-NsIM.

Substrates / EFs	2-NcIM	2-NsIM
Simulated	1.16×10^{9}	4.82×10^{4}
Experimental	$(3.08 \pm 0.07)\times10^{8}$	$(1.52 \pm 0.05)\times10^{3}$

area. The high consistence between experimental and the simulation results provides us a new path to investigate the various PC for SERS application via the simulation results.

Conclusions

This study investigates the effects of gap width and shape of silver nanoparticles positioned on the massed silver surface on the PC formation and the corresponding SERS responses. The redshift and intensity of PC increase with the decrease in the gap width of NcIM geometry. As for the shape effect of nanoparticles positioned on the massed silver surface, the stronger PC is induced under the λ_{max} laser irradiation for the parallel silver surface than the curve silver surface. In this case, 2-NcIM demonstrates the R6G characteristic peaks without noise signals in 10^{-9} M R6G solution. Meanwhile, 2-NcIM possesses respectively 2.06×10^4 and 2.41×10^4 times experimental and simulated EFs of 2-NsIM ($1.5 \pm 0.25\times10^4$ and 4.82×10^4), confirming the validity of the simulation results. In the future, novel SERS substrates with various PCs can be designed for the SERS application under different wavelength laser irradiation.

Experimental

Electromagnetic simulations by FDTD method. The FDTD program MEEP was used to perform the simulation [25]. The substrates assumed in the simulations are 50 nm Ag nanosphere / Ag nanocube atop the massed 80 nm thickness Ag surface with/ without a 2 nm dielectric spacer, which closely matched the SERS samples (in reality, 49.6 nm Ag nanosphere and 54.3 nm Ag nanocube). The excitation source was a linearly polarized radiation wave (polarized in the x-y plane). The grid size used for nanocube is 0.5 nm and that for nanosphere is 0.2 nm. The surrounding boundaries were the perfectly matched layers. The dielectric constant of silver used here was from the review (26). In absorption spectra, the EM field amplitude with/ without substrate is collected after a state function (30~300000 nm) EM wave excitation. Fourier transform is used to distinguish varying wavelength and the absorbance is calculated by the ratio of the EM field amplitude with substrate to that of background (without substrate). The maximum absorbance in absorption spectra is defined as λ_{max}. The EM field densities diagrams are calculated from the ratio of the EM field amplitude with substrate to that of background under λ_{max} (or 633 nm) EM wave excitation.

The preparation of SERS substrates. The synthesis of the Ag nanocubes and the nanospheres by chemical methods that offers good control over their shape is referenced from Xia [27]. The formation of silver nanocubes could be easily confirmed from tunnelling electron microscopy and the average size of silver nanocubes and nanospheres are 54.3 ± 1.45 nm and 49.6 ± 1.01 nm (the details are listed in Supporting information III). Ag surface was prepared by thermal evaporation of Ag (99.99% purity) onto the cleaned indium tin oxide substrates. To prepare a spacer on the substrates, Ag surface was soaked in the 0.1% 1, 2-ethanedithiol solution for 5 minutes with sonication and washed carefully to remove all unbonded 1, 2-ethanedithiol. Then, the Ag surface with a 1, 2-ethanedithiol monolayer was soaked in the Ag nanocubes /Ag nanospheres solution for 5 minutes with sonication. The substrates were cleaned several times by ethanol and sonicated to remove the unbonded nanoparticles.

Raman spectra. Raman spectra were taken by a confocal microscopic Raman spectrometer (In Via Raman microscope, RENISHAW, United Kingdom) using 633 nm radiation from the excitation of He–Ne laser. Before each measurement, Raman shift was calibrated by the signal of 520.7 cm^{-1} from a standard silicon wafer. The reported spectra were the results of a single 1 s accumulation in a range of 500–2000cm^{-1} and the characteristic R6G peak at 1360 cm^{-1} was selected to calculate the enhancement factor and the standard deviation from the average of 20 spectra in different sites.

Acknowledgements

Financial supports from National Science Council, Taiwan (Contract No. NSC 101-2221-E-006-227-MY3) and Headquarters of University Advancement, National Cheng Kung University, Taiwan (Contract No.D100-33B34) are acknowledged. The authors appreciate Prof. T.Y. Chen from National Tsinghua University, Taiwan for their valuable discussions and Mr. K. W. Tasi, doctorate student in Wen's group for his help in preparing manuscript.

Notes and references

[a] *Department of Chemical Engineering, National Cheng Kung University, Tainan, 70101, Taiwan. Fax: 886-6-2344496; Tel: 886-6-2385487; E-mail: tcwen@mail.ncku.edu.tw*

[b] *Department of Photonics, National Cheng Kung University, Tainan, 70101, Taiwan.*

[c] *Advanced Optoelectronic Technology Center, National Cheng Kung University, Tainan 70101, Taiwan.*

† Footnotes should appear here. These might include comments relevant to but not central to the matter under discussion, limited experimental and spectral data, and crystallographic data.

Electronic Supplementary Information (ESI) available: [details of any supplementary information available should be included here]. See DOI: 10.1039/b000000x/

1. H. Raether, *Surface Plasmons on Smooth and Rough Surfaces and on Gratings*, Berlin, Germany: Springer-Verlag, 1988.
2. S. A. Maier, *Plasmonics: Fundamentals and Applications*. NewYork: Springer-Verlag, 2007.
3. F.B. Arango, A. K. wadrin, A. F. Koenderink, *ACS Nano* 2012,**6**, 10156.
4. M. Tian, P. Lu, L. Chen, D. Liu, N. Peyghambarian, *Optics Communications,* 2012, **285** (24), 5122.
5. B. Huang, F. Yu, R. N. Zare, *Anal. Chem.,* 2007, **79**, 2979.
6. J. F. Li, X. D. Tian, S. B. Li, J. R Anema, Z.L. Yang, Y. Ding, Y. F. Wu, Y. M. Zeng, Q. Z. Chen, B. Ren, Z. L. Wang, Z. Q. Tian, *nature protocols*, 2013, **8** (1), 52.
7. H.J. Wu, J. Henzie, W. C. Lin, C. Rhodes, Z. Li, E. Sartorel, J. Thorner, P. Yang, *nature methods*, 2012, **9**(12), 1189.
8. S. Lin, W. Zhu, Y. Jin, Crozier K. B., *Nano Lett*., 2013, **13**, 559–563
9. J. B. Lassiter, F. McGuire, J. J. Mock, C. Ciracì, R. T. Hill, B. J. Wiley, A. Chilkoti, D. R. Smith, *Nano Lett.,* 2013, ***13***, 5866.
10. M. Yi, D. Zhang, P. Wang, X. Jiao, S. Blair, X. Wen, Q. Fu, Y. Lu, H. Ming, *Plasmonics*, 2011, **6**, 515.
11. F.J. Beck, A. Polman, K.R. Catchpole, *J. Appl. Phys.* 2009, 1**05,** 114310.

12. K. L. Wustholz, A.I. Henry, J. M. McMahon, R. G. Freeman, N. Valley, M. E. Piotti, M. J. Natan, G. C. Schatz, R.P. Van Duyne, *J. Am. Chem. Soc.,* 2010, **132** (31), 10903.
13. R. W. Taylor, R. J. Coulston, F. B. S., J. J. Baumberg, O. A. Scherman, *Nano Lett*., 2013, **13**, 5985.
14. Z. B. Wang, B. S. Luk'yanchuk, W. Guo, S. P. Edwardson, D. J. Whitehead, L. Li, Z. Liu, K. G. Watkins, *J. Chem. Phys*. 2008, **128** (9), 094705.
15. M. Futamata, Y. Maruyama, M. Ishikawa, *J. Phys. Chem. B*. 2003, 117.
16. N. Grillet, D. Manchon, F. Bertorelle, C. Bonnet, M. Broyer, E. Cottancin, J. Lerme´, M. Hillenkamp, M. Pellarin, *ACS Nano*, 2011, **5**, 9450.
17. E. Hao, G. C. Schatz, *J. Chem. Phys.* 2004, **120**, 357.
18. L. Li, T. Hutter, U. Steiner, S. Mahajan, *Analyst*, 2013,**138**, 4574-4578.
19. M. Rycenga, X. Xia, C. H. Moran, F. Zhou, D. Qin, Z. Y. Li, Y. Xia, *Angew. Chem. Int. Ed.,* 2011, **50** (24), 5473-5477.
20. N. S. Patrick, J. M. Catherine, *J. Phys. Chem. A*., 2009, **113**, 3973.
21. S.C. Cheng, T.C. Wen, *Materials Chemistry and Physics*, 2014,**143**, 1331-1337
22. K. D. Alexander, K. Skinner, S. Zhang, H. Wei, R. Lopez, *Nano Lett.*, 2012, **10**, 4488.
23. S. Y. Lee, L. Hung, G. S. Lang, J. E. Cornett, I. D. Mayergoyz, O. Rabin, *ACS Nano*, 2010,**4** (10), 5763.
24. J. O. Christopher, G. Anand, K. S. Tapan, J. M. Catherine, *Anal. Chem.*, 2005, **77**, 3261.
25. S. Mubeen, S. Zhang, N. Kim, S. Lee, S. Krämer, H. Xu, M. Moskovits, *Nano Lett*., 2012, **12**, 2088−2094.
26. S. Astilean, Ph. Lalanne, M. Palamaru, *Opt. Commun*., 2000, **175**, 265-273.
27. Y. Sun, Y. Xia, *Science*, 2002, **298**, 2176.